SAND2019-3833C

Proceedings of the ASME 2019 Pressure Vessels & Piping Conference
PVP 2019
July 14-19, 2019, San Antonio, TX, USA

PVP2019-93823

EVALUATING THE RESISTANCE OF AUSTENITIC STAINLESS STEEL WELDS TO HYDROGEN EMBRITTLEMENT

Joseph Ronevich[1], Chris San Marchi, Dorian K. Balch
Sandia National Laboratories
Livermore, CA, USA

ABSTRACT

Austenitic stainless steels are used extensively in hydrogen gas containment components due to their known resilience in hydrogen environments. Depending on the conditions, degradation can occur in austenitic stainless steels but typically the materials retain sufficient mechanical properties within such extreme environments. In many hydrogen containment applications, it is necessary or advantageous to join components through welding as it ensures minimal gas leakage, unlike mechanical fittings that can become leak paths that develop over time. Over the years many studies have focused on the mechanical behavior of austenitic stainless steels in hydrogen environments and determined their properties to be sufficient for most applications. However, significantly less data have been generated on austenitic stainless steel welds, which can exhibit more degradation than the base material. In this paper, we assess the trends observed in austenitic stainless steel welds tested in hydrogen. Experiments of welds including tensile and fracture toughness testing are assessed and comparisons to behavior of base metals are discussed.

NOMENCLATURE

a	=	crack length, precrack length
a/W	=	crack length/width
B, B_N	=	specimen thickness: actual, effective
b_o	=	remaining ligament
CT	=	compact tension
DIC	=	digital image correlation
DCPD	=	direct current potential difference
EBW	=	electron beam weld
FN	=	ferrite number
GTAW	=	gas tungsten arc weld
J_H	=	subcritical cracking threshold
K	=	stress intensity factor
K_{JH}	=	size independent plane-strain fracture
S_Y	=	average of yield and tensile strength
W	=	width

INTRODUCTION

Over the years, studies have been completed to assess the performance of austenitic stainless steels to hydrogen embrittlement [1-3]. In general, despite some degradation due to hydrogen, austenitic stainless steels maintain mechanical properties superior to many other alloy classes and thus, through proper design, have been utilized in many applications. There has been significantly less research performed on welds, but growing interest in the performance of welds to reduce the number of mechanical joints and leaks associated with the joints. It is commonly assumed that welds behave significantly poorer than the parent metals, which has likely led to the limited use of welding in hydrogen infrastructure. While more research

[1] Contact author email: jaronev@sandia.gov

is needed to improve our understanding of the performance of welded austenitic stainless steels for applications in gaseous hydrogen, numerous studies have shown that, like wrought austenitic stainless steel, welded austenitic stainless steels behave well in hydrogen environments.

In this work, tensile testing and fracture toughness measurements were performed on welds fabricated using two different welding techniques (gas tungsten arc weld (GTAW) and electron beam welding (EBW)). The results from non-charged and hydrogen-precharged are compared. The discussion includes comparisons to other weld results from the literature.

EXPERIMENTAL PROCEDURES

Materials

A 304L stainless steel was examined in this study, which was high-energy rate forged at 843 °C (1550 °F) into a cylinder resulting in yield strength of 423 MPa. Weld rings were machined from the forgings with features to join two rings either by gas tungsten arc weld (GTAW) or electron beam weld (EBW). The joint design is necessarily different for these two weld practices, and in order to accommodate the different test specimen geometries used, the joint rings had different outer diameters: 81 mm for the EBW and 76 mm for the GTAW. A 308L filler metal was used for the GTAW and the composition can be found in Table 1 along with the composition of the 304L parent metal. The groove depth was nominally 10 mm and 6 continuous passes were used to fill the groove. The EBW is an autogenous weld and therefore no filler metal is added. The welding parameters are listed in Table 2. Images are shown in Fig. 1 for the two welds investigated in this study: GTAW and EBW. The nominal microstructure consists of skeletal ferrite (thin grey regions) in an austenite matrix (white), although each welding process develops a distinct morphology as a result of the heat input. The GTAW consists of multiple weld passes and the resulting solidification direction is apparent in Fig. 1. Along the centerline, the dendrites extend predominantly from weld root to cover pass (e.g. from bottom to top in Fig. 1). The EBW has significantly finer solidification structures and also exhibits more random orientations. The overall heat input is much less in the EBW resulting in faster solidification and finer features.

Ferrite content of the welds was measured using a Feritescope® and found to increase in both welds from inner to outer diameter of the welded ring. Reported values are those measured near the central region of the weld on the fracture test coupons, near the region of the precrack terminus, approximately at the middle of the specimen. Average ferrite numbers (FN) in this location are 3.5 in the 304L EBW and 5.6 in the GTAW [4]. At low values (<10), FN can be assumed equivalent to percent ferrite.

Round tensile specimens were removed perpendicular to the EBW direction where the weld was located in the center of gage section. A gage section of 25 mm was used with a diameter of 4 mm. Flat tensile specimens were removed from GTAW with a gage section entirely contained within the weld. The gage section of these GTAW tensile specimens was 3.5 mm with a cross section of 0.76 mm x 0.63 mm as reported previously in [4].

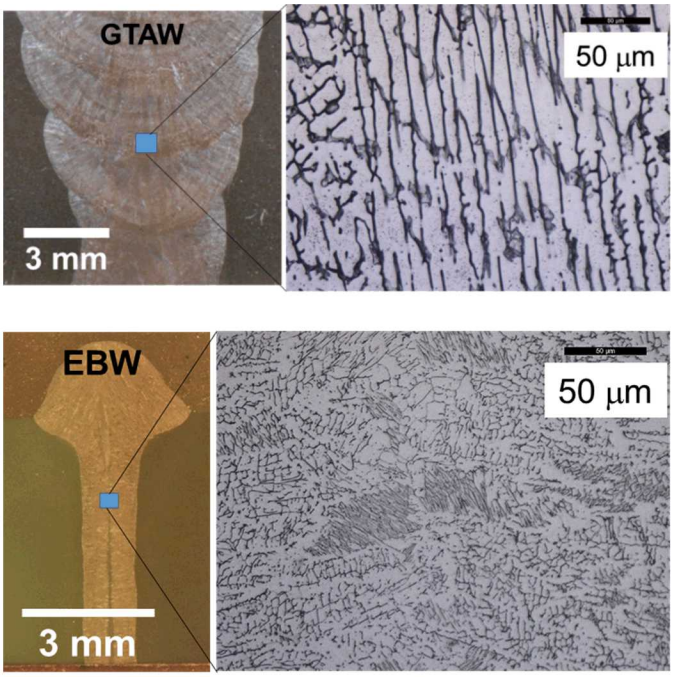

Figure 1 - Optical images of 304L GTAW and EBW at low and high magnification.

Fracture toughness specimens were machined from the weld rings in two different geometries. Three-point bend bars were removed from the GTAW rings and arc specimens were removed from the EBW rings. Drawings of the specimen geometries are shown in Fig. 2. In both specimens, the notches were positioned in the center of the weld with cracks growing radially from inner diameter to outer diameter of the ring, with axial loading (i.e., LR orientation). Side grooves were machined on the specimens in accordance with ASTM E1820 [5] to ensure crack uniformity and constraint was maintained at the crack.

Specimens were fatigue precracked to a crack length (a/W) of approximately 0.5 and subsequently hydrogen-precharged to approximately 140 wppm H by thermal precharging at temperature of 300°C in gaseous hydrogen at pressure of 138 MPa for approximately 2 weeks.

Specimens were removed from the thermal precharging system and stored in a freezer at 218 K to limit hydrogen egress prior to testing.

Tensile Testing

Tensile testing was accomplished via constant actuator displacement, corresponding to an average strain rate of 3.3 x 10^{-4} s^{-1}. A laser extensometer was used on the flat tensile specimens and digital image correlation (DIC) was used on the round bars to measure strain. Following the experiments, reduction of area was measured.

Rising Displacment Fracture Toughness Testing

Rising displacement fracture toughness tests were performed on bend bars and arc specimens in the hydrogen -precharged condition. Tests were performed according to ASTM E1820 [5] under actuator displacement control. The arc geometry is described in ASTM E399 [6], but an elastic-plastic analysis was performed consistent with E1820 [5]. Displacement rates ranged from 0.12 to 15 mm/hr. Direct current potential difference (DCPD) was employed to monitor crack positions according to ASTM E1737-96 [7]. J vs Δa curves (e.g. J-R curves) were generated from load, displacement, and DCPD data according to ASTM E1820 [5]. Tests were terminated when the DCPD signal increased above background by at least 15%. Following the fracture test, specimens were heat tinted at 350°C for 1 hr to mark the end of the fracture test. Fatigue loading was then applied to the specimen to separate the cracks and allow examination of fracture surfaces. The subcritical cracking threshold (J_H) values were determined via the intersection of the 0.2 mm offset construction line with the J-R curve. When specific dimensions are met, J_H can represent a size independent plane-strain fracture parameter according to ASTM E1820 [5]. These requirements are as follows

$$B > (10*J_H)/S_Y \text{ and } b_o > (10*J_H)/S_Y \quad (1)$$

where B is thickness, S_Y is effective yield strength (average of yield and ultimate tensile strength), and b_o is remaining uncracked ligament. Due to the high J_H values in this study, the criteria is often violated for thickness, therefore the results may not be size independent. However, testing of the 304L base metal was performed using 3 different specimen geometries (compact tension, 3-point bend, and arc) which yielded similar J_H values suggesting minimal size/geometry dependence.

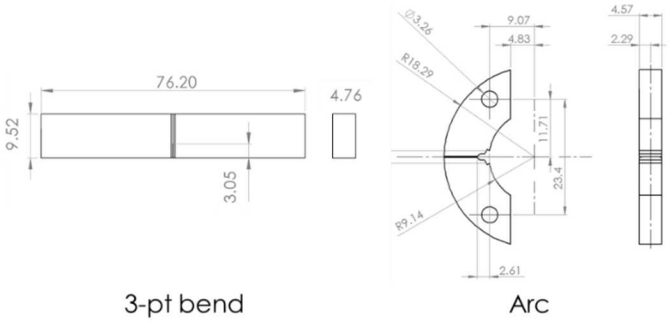

Figure 2 – Schematic drawing of 3-pt bend bar and arc specimen. Units are in mm.

RESULTS

Tensile testing

Duplicate tensile tests were performed in the non-charged and hydrogen-precharged condition on the EBW. The results showed good repeatability for the reduction of area (RA) for the EBW as shown in Table 3. The average RA for the non-charged EBW was 0.88 and for the hydrogen-precharged EBW was 0.50. The RA for the 304L BM was 0.85 for the non-charged and 0.40 for the hydrogen-precharged condition. The GTAW exhibited a RA of 0.82 for the non-charged and 0.58 for the hydrogen-precharged. All of the samples exhibited a RA greater than 0.40 in the hydrogen-precharged condition with the welds having higher RA than the base metals. A comparison to the broader body of literature data is described in the discussion section.

Subcritical Cracking Thresholds (J_H)

The J_H values are plotted for the 304L forged base metal, 304L GTAW, and 304L EBW in Fig. 3 as a function of the testing rate as expressed in units of dK/dt (change in K as function of time in the elastic loading part of J-R curve). The open symbols represent the base metal (BM) forgings and the closed symbols represent the welds. Three different specimen geometries are shown in Fig. 3 for the 304L BM: 3-pt bend, Arc, and compact tension (CT) [3]. The results show that J_H values for the base metal (BM) appear similar regardless of specimen geometry or testing rate (dK/dt) and exhibit an average J_H value of 241 kJ/m^2. The results from the EBW exhibit similar J_H values with an average of 237 kJ/m^2. The GTAW exhibits lower J_H with an average of 128 kJ/m^2. The welds exhibit more sensitivity to testing rate than the base metals; however, for this paper, the results for all testing rates are averaged to simplify comparisons. A more detailed discussion on geometry and testing rate effects can be found in [4].

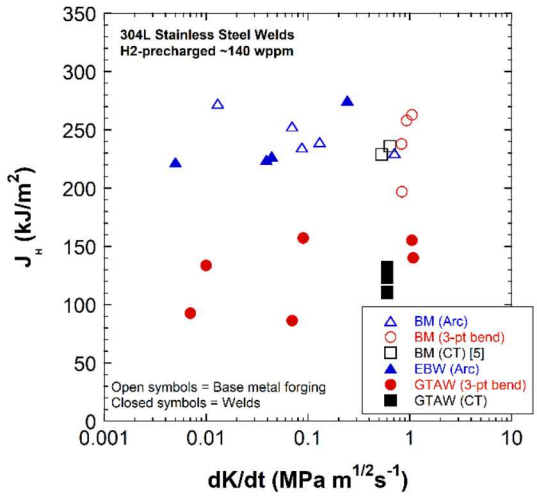

Figure 3 – J_H vs dK/dt of 304L BM, GTAW, and EBW in hydrogen-precharged condition. Note that the results using the CT specimens are from [3].

Fracture Surface Evaluation

Following completion of the fracture tests, the fracture surfaces were examined using scanning electron microscopy to examine features unique on the fracture surfaces. The fracture surfaces are shown in Fig. 4 for the GTAW and EBW. In all images in Fig. 4 the crack propagation direction is from bottom to top and there are distinct regions representing the precrack, fracture test, and overload or post-fatigue region which was used to break the specimen in half. On the GTAW fracture surface, dendritic features are prevalent and run parallel to the crack propagation direction. As was shown in Fig. 1, the center of the GTAW has a solidification structure dominated by dendrites aligned parallel to the crack propagation direction at the weld centerline. Conversely, the etched weld microstructure of the EBW shows a noticeable absence of any elongated dendrites in Fig. 1. The fracture surface of the EBW also shows no signs of dendritic features. The fracture features observed in the EBW are more typical of what is observed in base metal (not shown in this paper) which are a mixture of microvoids and regions of shear. The coarser dendritic features observed in the GTAW appear to influence the fracture path more than in the EBW where the ferrite is finer.

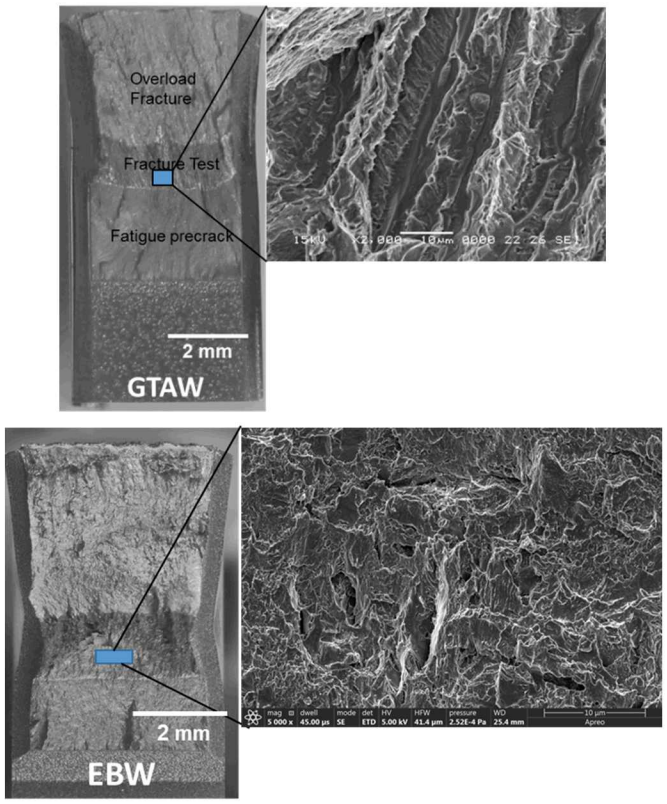

Figure 4 – Fracture surfaces of GTAW from 3-pt bend specimen, and EBW from arc specimen.

DISCUSSION

The experimental work presented in this paper was focused on two welds (GTAW and EBW) compared to their parent forged 304L base material. Following hydrogen-precharging, a loss of reduction of area (RA) was observed in all three materials with the base metal exhibiting the greatest loss of RA from 0.85 to 0.4, a 54% reduction. The GTAW and EBW exhibited smaller reductions of RA in hydrogen precharged condition than the BM. Despite the decreases of RA with hydrogen, the RA values are still quite high at greater than 0.4 demonstrating that significant ductility is retained in all three of these materials when saturated with hydrogen.

The subcritical cracking threshold, J_H, was also observed to be degraded with hydrogen although thresholds of the 304L BM and EBW were greater (241 and 237 kJ/m^2, respectively) than the 304L GTAW (128 kJ/m^2). In order to provide a broader comparison of austenitic stainless steel weld behavior in hydrogen precharged conditions, hydrogen-precharged RA and J_H data from the literature are included in this discussion.

Reduction of Area

Figure 5 shows a summary of RA for a variety of austenitic stainless steel base metals and welds from the literature [2, 4, 8-10] which were subjected to thermal gaseous hydrogen-precharging prior to testing. In Fig. 5, the RA in the non-charged and hydrogen-precharged conditions are shown tested at ambient conditions. In select materials, the results are shown for tests performed at -50°C. Because multiple 304L GTAWs are discussed, the different 304L GTAW are distinguished by using the first letter of the author's last name following the material, such as 304L-Y, GTAW-B, or GTAW-Y. The exception is the autogeneous orbital tube welds from Ref. [8], which are designated as 316L GTAW A and 316L GTAW B consistent with the designations from the original publication.

The base metal alloys of 304L-Y show RA with hydrogen as low as 0.32 and the 316L show RA as low as 0.46. These represent losses of RA with hydrogen ranging from 14% to 54%. The role of composition, specifically increased Ni-content, appears to improve the ductility in the hydrogen-precharged condition of the 316L base metals [2]. Low temperature environments (-50°C) further reduce RA in hydrogen-precharged condition of 304L base metal to below 0.2. All of the base metals assessed are affected by hydrogen but retain RA greater that 0.32 at room temperature.

A variety of weld data are shown in Fig. 5 of different austenitic stainless steels as well as different welding techniques: GTAW and EBW. In general, in the hydrogen-precharged condition, the RA of the 316L welds remains the highest compared to the 304L and 21-6-9 welds. This is consistent with the 316L BM exhibiting higher RA compared to the 304L BM when hydrogen-precharged. All of the 316L weld data exhibited an RA greater than 0.4 following hydrogen precharging. The 316L welds examined were all fabricated using GTAW although some parts were tubes as indicated in Fig. 5.

Two different welding techniques (e.g. GTAW and EBW) are compared on 304L welds which exhibit a variety of RA values following hydrogen-precharging. The lowest measured RA was on a 304L GTAW-Y [9] with a RA of 0.12; however, it should be noted that the RA in air was uncharacteristically low at 0.34 compared to the other 304L GTAW and 304L GTAW-B [10] which ranged from 0.77 to 0.83. The base metal of the 304L GTAW-Y also had slightly lower ductility with an RA of 0.62 in air and 0.32 in hydrogen, suggesting that the quality of the BM was lower than typical of this grade of steel and influenced the dutility when welded. The lower ductility of the 304L GTAW-Y material was attributed to high ferrite content nearing 8%. An EBW-Y was fabricated from this same alloy [9] which exhibited greater resistance in the hydrogen precharged condition (RA = 0.29) which was comparable to its 304L BM-Y RA value (RA = 0.32). The 304L EBW-Y [9] contained only 1% ferrite.

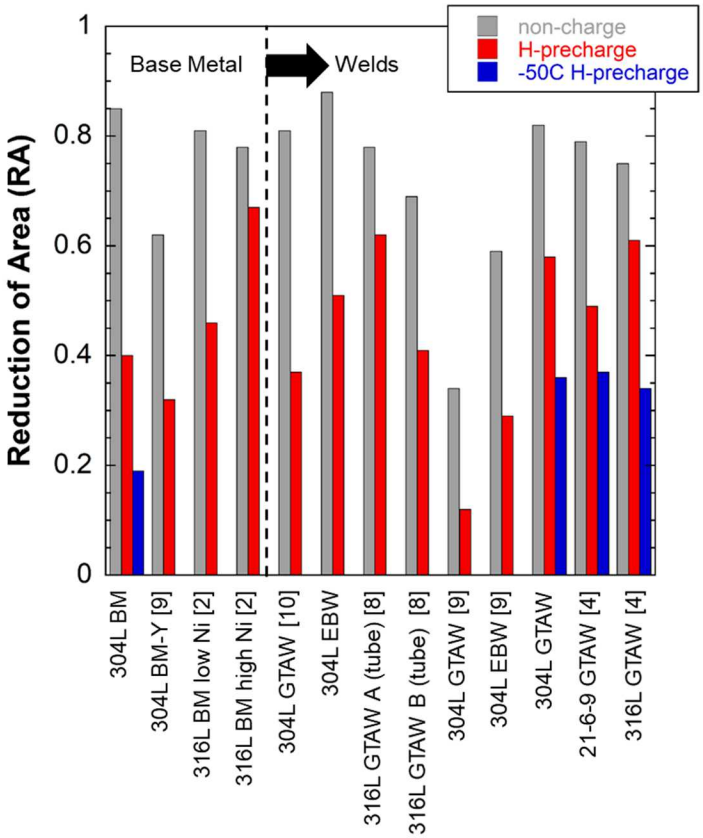

Figure 5 – Summary of RA for welds in literature and select base metals. For the 316L base metals low Ni is 10.25% and high Ni is 13.5% [2]. Data taken from [2, 4, 8-10].

The influence of low temperature was assessed in previous work on GTAW [4] in terms of the total elongation. The RA for the GTAW tested at -50°C were measured on those specimens and are shown in Fig. 5 for 304L, 21-6-9, and 316L welded with 308L. The results show a further decrease of RA when tested at -50°C following hydrogen charging, which is consistent with the literature on base metals [2, 11]. This trend is similar to the 304L BM tested, although the welds retain higher RA than the 304L BM.

Fracture thresholds

The subcritical cracking threshold, J_H, measurements on hydrogen-precharged materials are shown in Fig. 6 for the current 304L BM, GTAW, and EBW compared to data from the literature. Subcritical cracking threshold, J,

measurements for the non-charged conditions are not shown because often times no detectable crack propagation was observed. Results in the form of J_H are shown for tests completed at 293K and in some cases 223 K. Error bars represent the standard deviation and are shown when this value could be calculated. The standard deviation is meant to include variability from multiple tests or due to different testing rates. The influence of testing rate was discussed previously in [4]. Three different base metals are shown which all have comparable J_H values: 304L BM and two heats of 21-6-9 BM with initial ferrite contents of 0 (low ferrite) and 2% (high ferrite), respectively [12].

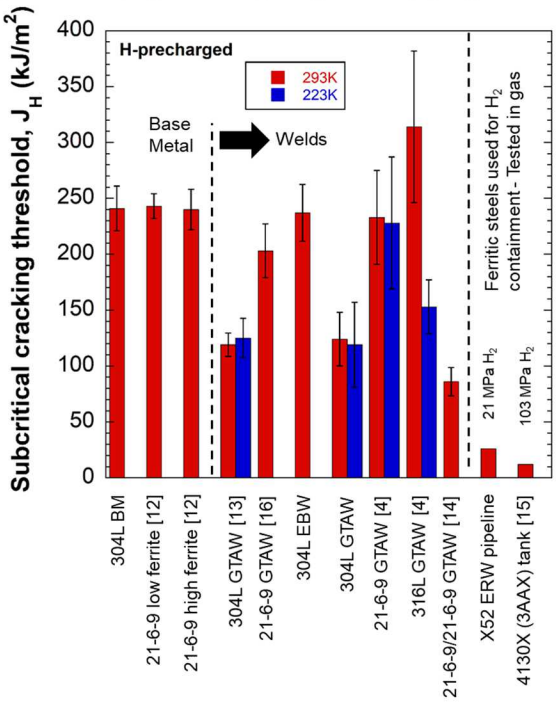

Figure 6 – Summary of J_H values for different austenitic stainless steel welds in hydrogen-precharged condition. Results are shown for tests performed at 293 and 223 K. J_H values for an X52 ERW pipeline and 4130X steel are shown for reference. Data taken from [4, 12-16].

On average, the welds exhibit a reduction in J_H compared to the base metal. For example measurements from two different studies on 304L GTAW and 304L GTAW-J [13] show nearly a 50% reduction in J_H compared to the parent metal. However, the 304L EBW and 21-6-9 GTAW [4] show almost no difference in J_H compared to the base metals. The 316L GTAW [4] shows very high toughness when tested at 293 K, however, a reduction of nearly 50% was observed when tested at low temperatures of 223 K. The other three welds which were tested at low temperature exhibited negligible temperature effects [4]. The final austenitic stainless steel weld shown is 21-6-9/21-6-9 GTAW [14] which exhibited the lowest measured J_H of the stainless steel welds compared here. It is worth noting that the average ferrite content in the 21-6-9/21-6-9 GTAW was over 7%. The ferrite contents of the other tested GTAW (e.g. 304L, 21-6-9, and 316L, all fabricated with 308L filler metal) were between 3.8 and 5.6% ferrite [4].

In addition to the austenitic stainless steel base metal and welds, two ferritic based materials are shown to provide perspective on the performance in hydrogen gas. The first is an X52 electric-resistance weld (ERW) pipeline steel which is a material used to transport hydrogen gas and was tested in 21 MPa H_2 (publication in progress). The second is a 4130X [15] (e.g. 3AAX) quenched and tempered Cr-Mo steel which is the predominant material found in laboratory gas cylinders that contain high pressure hydrogen gas. The 4130X steel was tested in 103 MPa H_2. The X52 ERW had a J_H of 30 kJ/m^2 and the 4130X had a J_H of 12 kJ/m^2. A comparison of the J_H thresholds of the ferritic steel to the austenitic stainless steel base metals and welds emphasizes two important conclusions: 1) austenitic stainless steels are the material of choice for high pressure hydrogen containment because they show much greater subcritical fracture threshold in gaseous hydrogen than ferritic steels, and 2) while the subcritical fracture threshold of austenitic stainless steel welds is reduced due to hydrogen, the J_H values are often similar to the base materials and always substantially greater than ferritic steels (e.g. X52 and 4130X) that are commonly used to store high pressure hydrogen.

Role of Ferrite

The observation that increasing ferrite reduces J_H has been noted in the literature before by Jackson *et al.* [16]. In the current study, the assessed welds have a variety of ferrite contents and therefore the subcritical cracking threshold, J_H, results from this paper are compared to the results from [16] as a function of ferrite content. In addition, the influence of ferrite on RA is discussed below for hydrogen-precharged welds.

In a study on 304L EBW-Y and GTAW-Y in the literature [9], the ferrite content differed significantly (8% and 1% for GTAW-Y and EBW-Y, respectively). For these two welds [9] the RAs were 0.12 and 0.29 for the GTAW-Y (8% ferrite) and EBW-Y (1% ferrite), respectively. In the present study, the RA values for the 304L GTAW (5.6% ferrite) and EBW (3.5% ferrite) were 0.58 and 0.50, respectively, showing no correlation between ferrite and RA. To examine this more broadly, Fig. 7 was developed to show RA as a function of FN (e.g. ferrite content). This is the ferrite content prior to the test and therefore does not

include any martensite formation that may have formed during deformation. The RA does not appear to follow any specific trend with ferrite content. At the higher ferrite content of 8%, the RA is low but at ferrite contents below this there seems to be no real influence of ferrite.

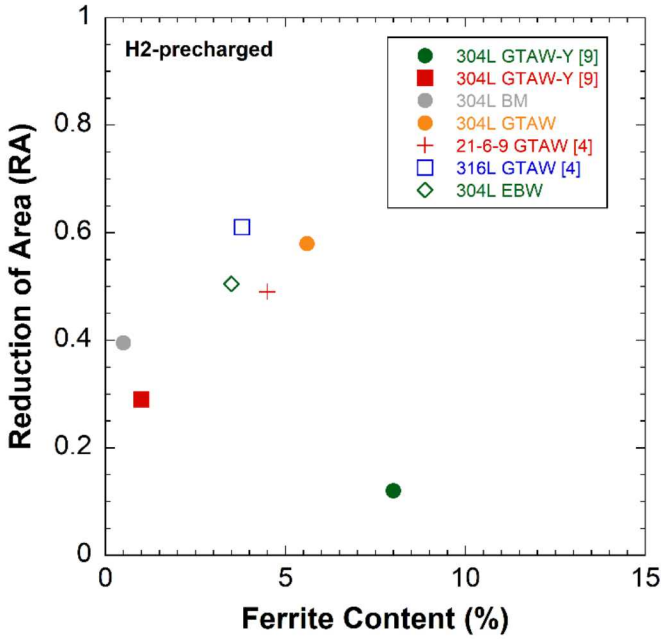

Figure 7– Reduction of area from tensile tests on hydrogen-precharged stainless steels as a function of ferrite content. Data taken from [4, 9].

Values of the fracture threshold J_H as a function of ferrite are plotted in Fig. 8 similar to previous work by Jackson *et al*. [16]. There are welds data in the literature with ferrite contents up to 33% [17]. The addition of the welds tested in this study (304L EBW and 304L GTAW) follow the trends observed by Jackson *et al*. [16] which is increasing ferrite results in lower J_H when hydrogen-precharged. As discussed previously [16], the ferrite forms during solidification and provides lower resistance to crack nucleation and propagation. In GTAW, the dendrites are large and parallel to the solidification direction (which happen to be parallel to the crack propagation direction in the experiments). The fracture surfaces of 304L GTAW fracture toughness tests show distinct dendritic features running parallel to the crack propagation direction as shown in Fig. 4. In EBW, the overall heat input is lower and therefore the microstructure has finer features and an absence of long-range dendiritic directionality, as shown in Fig. 1. This appears to affect the fracture pathway as shown in Fig. 4, where there is a lack of these dendritic features on the fracture surface in the 304L EBW. The finer solidication structure, lower ferrite content, and lack of long dendritic features all seem to improve the toughness of 304L EBW compared to the GTAW in the hydrogen-precharged condition.

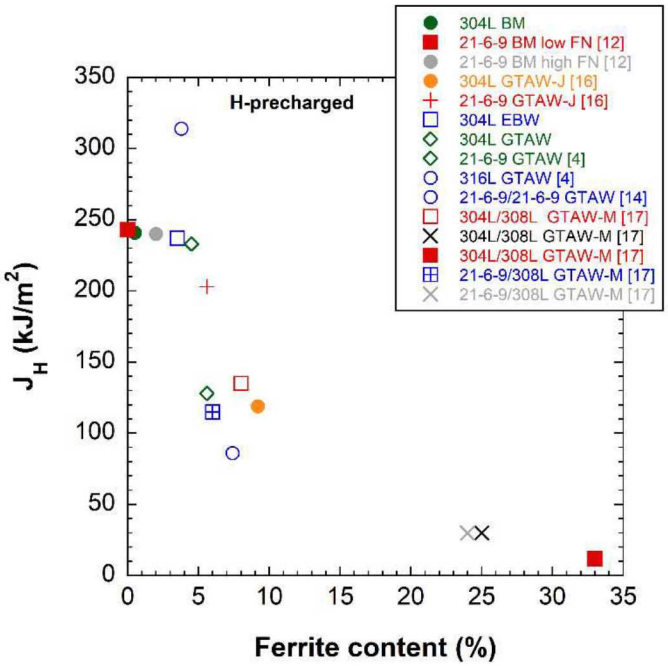

Figure 8– Subcritical crack threshold, J_H, for hydrogen precharged stainless steel welds as a function of ferrite content. This figure was modified from [16] and includes data from [4, 12, 16, 17].

Role of Nickel Content

The role of nickel has been observed to correlate with improved reduction of area in hydrogen precharged wrought stainless steels [18, 19]. Figure 9 shows a plot of RA versus nickel content for select wrought 304L and 316L precharged stainless steels ranging from 8 to 13.5% nickel. In the absence of hydrogen, the RA remains approximately at 0.8 regardless of nickel content. Following hydrogen precharging, the RA decreases as nickel content decreases. Hydrogen precharged stainless steel welds discussed in Fig. 5 of this paper are shown in Fig. 9. The welds appear to follow a similar trend as the wrought metals. Even the welds tested at 223 K show only a slightly lower RA compared to the wrought metals. The weld [9] (noted by arrow) showing a particularly low RA was identified as having very high ferrite contents (8%) which may account for the poor RA.

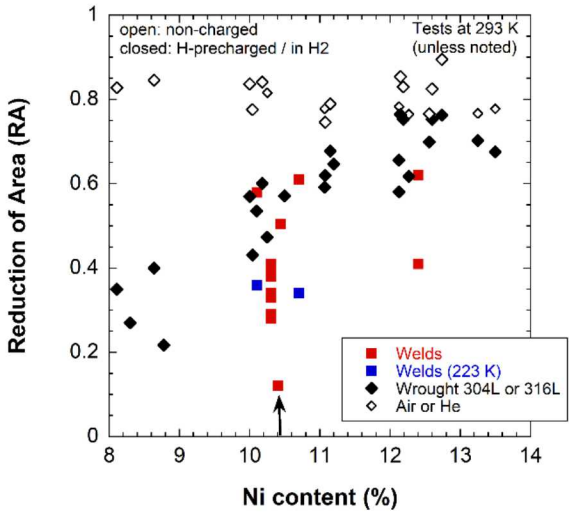

Figure 9 – Reduction of area for a variety of wrought 304L and 316L metals either precharged with hydrogen on in high pressure hydrogen gas tested at 293 K compared to precharged austenitic stainless steel welds at 293 K and 223 K. Also shown are wrought 304L or 316L tested in non-charged condition in air or He. Refs [4, 9, 10, 18, 19].

SUMMARY

Two different austenitic stainless steel welds were fabricated from forged 304L: gas tungsten arc weld (GTAW) and electron beam weld (EBW). Test coupons were removed from the welds and thermally precharged with hydrogen gas followed by tensile and J_H testing in air at room temperature. Results were compared to the parent base metal (BM). The results showed that the reduction of area (RA) was greater than the parent 304L metal in the hydrogen-precharged conditions and that all three materals (304L BM, GTAW, and EBW) had measured RA > 0.4.

The fracture threshold of the 304L GTAW displayed lower values than the 304L EBW when hydrogen-precharged. The 304L EBW exhibited comparable J_H values to the parent BM. A comparison of microstructures shows that the EBW possesses finer microstructural features and fewer dendrites extending parallel to crack direction, likely due to lower heat input in the EBW. The higher ferrite content and alignment of dendrites parallel to crack propagation direction enhance the effects of hydrogen-precharging on the GTAW, in comparison to the EBW. Long dendritic features, for example, were observed on the fracture surface of the GTAW but were absent on the EBW.

Comparisons were made between the RA and J_H results of the current study and the literature. A trend was observed with increasing nickel content resulting in improved RA in hydrogen precharged condition. This trend was consistent with wrought metals and welds. Ferrite found in austenitic stainless steel welds appears to affect J_H more than it affects RA. However, despite the effects of hydrogen on RA and J_H, austenitic stainless steel welds retain high ductility and toughness compared to other common materials of construction for high pressure hydrogen gas containment.

ACKNOWLEDGMENTS

The authors are grateful to J. Campbell and B. Davis for support of high pressure testing, A. Gardea, H.Vega for metallographic preparation, and W. York and R. Nishimoto for SEM imaging. Additionally, thanks to H. Jin and K. Nelson for EBW tensile testing with DIC. Sandia National Laboratories is a multimission laboratory managed and operated by National Technology and Engineering Solutions of Sandia, LLC., a wholly owned subsidiary of Honeywell International, Inc., for the U.S. Department of Energy's National Nuclear Security Administration under contract DE-NA-0003525.

TABLE 1 – CHEMICAL COMPOSITIONS

Material	Fe	Cr	Ni	Mn	Si	C	N	P	S	Yield Strength (MPa)
304L	Bal.	19.38	10.44	1.72	0.57	0.027	0.02	0.021	0.002	423
308L Filler	Bal.	20.5	10.3	1.56	0.50	0.028	0.055	0.006	0.012	N/A

TABLE 2 – WELD PARAMETERS OF EBW AND GTAW

Parameters	EBW	GTAW
Voltage	140 kV	9.4
Current	41 mA	205
Travel speed	76.2 cm/min	6.3
Notes:	• 24 s (1 s upslope, 1 s downslope) • Sharp focus +20 mA (sharp focus at 850 mA)	• Ar shield gas flow rate 0.85 Nm^3/h • Filler wire feed rate = 74 cm/min

TABLE 3 - TENSILE PROPERTY RESULTS FROM GTAW AND EBW

	Reduction of Area (RA)	
Material	**non-charged**	**H-charged**
Base Metal	0.85	0.40
EBW	0.88 / 0.89	0.50 / 0.51
GTAW	0.82	0.58

REFERENCES

[1] C. San Marchi, D. K. Balch, K. A. Nibur, and B. P. Somerday, "Effect of High-Pressure Hydrogen Gas on Fracture of Austenitic Steels," *Journal of Pressure Vessel Technology,* vol. 130, pp. 1-9, 2008.

[2] C. San Marchi, B. P. Somerday, X. Tang, and G. H. Schiroky, "Effects of alloy composition and strain hardening on tensile fracture of hydrogen-precharged type 316 stainless steels," *International Journal of Hydrogen Energy,* vol. 33, no. 2, pp. 889-904, 2008.

[3] H. Jackson, C. San Marchi, D. Balch, B. Somerday, and J. Michael, "Effects of Low Temperature on Hydrogen-Assisted Crack Growth in Forged 304L Austenitic Stainless Steel," *Metallurgical and Materials Transactions A,* journal article vol. 47, no. 8, pp. 4334-4350, August 01 2016.

[4] J. Ronevich, C. San Marchi, and D. K. Balch, "Temperature effects on fracture thresholds of hydrogen precharged stainless steel welds PVP2017-65603," presented at the ASME 2017 Pressure Vessels & Piping Conference, Waikoloa, HI, 2017.

[5] *E1820-11 Standard Test Method for Measurement of Fracture Toughness*, 2011.

[6] *E399 Standard Test Method for Linear-Elastic Plane-Strain Fracture Toughness K_{IC} of Metallic Materials*, 2012.

[7] *E1737-96 Standard Test Method for J-Integral Characterization of Fracture Toughness*, 1996.

[8] L. A. Hughes, B. P. Somerday, D. K. Balch, and C. San Marchi, "Hydrogen compatibility of austenitic stainless steel tubing and orbital tube welds," *International Journal of Hydrogen Energy,* vol. 39, no. 35, pp. 20585-20590, 2014/12/03/ 2014.

[9] C. M. Younes, A. M. Steele, J. A. Nicholson, and C. J. Barnett, "Influence of hydrogen content on the tensile properties and fracture of austenitic stainless steel welds," *International Journal of Hydrogen Energy,* vol. 38, no. 11, pp. 4864-4876, 2013/04/15/ 2013.

[10] D. K. Balch and C. San Marchi, "Effect of hydrogen on tensile strength and ductility of multi-pass 304L/308L austenitic stainless steel welds PVP2015-45591," presented at the ASME 2015 Pressure Vessels and Piping Conference, Boston, MA, 2015.

[11] M. R. Louthan Jr, G. R. Caskey Jr, J. A. Donovan, and D. E. Rawl Jr, "Hydrogen embrittlement of metals," *Materials Science and Engineering,* vol. 10, pp. 357-368, 1972.

[12] K. A. Nibur, B. P. Somerday, D. K. Balch, and C. San Marchi, "The role of localized deformation in hydrogen-assisted crack propagation in 21Cr–6Ni–9Mn stainless steel," *Acta Materialia,* vol. 57, no. 13, pp. 3795-3809, 2009.

[13] H. F. Jackson, C. San Marchi, D. K. Balch, and B. P. Somerday, "Effect of low temperature on hydrogen-assisted crack propagation in 304L/308L austenitic stainless steel fusion welds," *Corrosion Science,* vol. 77, no. 0, pp. 210-221, 2013.

[14] B. P. Somerday, M. Dadfarnia, D. K. Balch, K. A. Nibur, C. H. Cadden, and P. Sofronis, "Hydrogen-Assisted Crack Propagation in Austenitic Stainless Steel Fusion Welds," *Metallurgical and Materials Transactions A,* vol. 40, no. 10, pp. 2350-2362, 2009.

[15] K. Nibur, B. Somerday, C. Marchi, J. Foulk, III, M. Dadfarnia, and P. Sofronis, "The Relationship Between Crack-Tip Strain and Subcritical Cracking Thresholds for Steels in High-Pressure Hydrogen Gas," (in English), *Metallurgical and Materials Transactions A,* pp. 1-22, 2012/11/01 2012.

[16] H. F. Jackson, K. A. Nibur, C. San Marchi, J. D. Puskar, and B. P. Somerday, "Hydrogen-assisted crack propagation in 304L/308L and 21Cr–6Ni–9Mn/308L austenitic stainless steel fusion welds," *Corrosion Science,* vol. 60, no. 0, pp. 136-144, 2012.

[17] M. J. Morgan, G. K. Chapman, M. H. Tosten, and S. L. West, "Tritium Effects on Fracture Toughness of Stainless Steel Weldments," presented at the Trends in Welding Research: Proceedings of the 7th International Conference, Pine Mountain, GA, USA, 2005. Available: http://www.osti.gov/scitech//servlets/purl/881343-4DYxAQ/

[18] C. S. Marchi and B. P. Somerday, "Comparison of stainless steels for high-pressure hydrogen service PVP2014-28811," presented at the ASME Pressure Vessels and Piping Division Conference, Anaheim, CA, 2014.

[19] N. T. Switzner *et al.*, "Hydrogen-assisted fracture in forged type 304L austenitic stainless steel," presented at the 2012 International Hydrogen Conference, Moran, WY, 2012.